Colloids and Surfaces A 554 (2018) 306–316

Contents lists available at ScienceDirect

Colloids and Surfaces A

journal homepage: www.elsevier.com/locate/colsurfa

Analysis of stability behavior of carbon black nanoparticles in ecotoxicological media: Hydrophobic and steric effects

Gukhwa Hwang[a,b], Allan Gomez-Flores[a], Scott A. Bradford[b], Sowon Choi[a], Eunhye Jo[c], Song Bae Kim[e], Meiping Tong[f], Hyunjung Kim[a,b,*]

[a] Department of Mineral Resources and Energy Engineering, Chonbuk National University, Jeonju, Jeonbuk 54896, Republic of Korea
[b] US Salinity Laboratory, USDA, ARS, Riverside, CA, USA
[c] Risk Assessment Division, National Institute of Environmental Research, Hwangyeong-ro 42, Seo-gu, Incheon 22689, Republic of Korea
[e] Department of Rural Systems Engineering, Seoul National University, Republic of Korea
[f] The Key Laboratory of Water and Sediment Sciences, Ministry of Education, College of Environmental Sciences and Engineering, Peking University, Beijing 100871, China

GRAPHICAL ABSTRACT

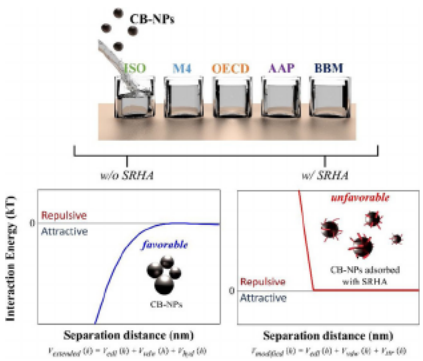

ARTICLE INFO

Keywords:
Carbon black nanoparticles
Ecotoxicological medium
Stability
Hydrophobic force
Steric force

ABSTRACT

The stability of carbon black nanoparticles (CB-NPs) was investigated in five different ecotoxicity test media for fish, daphnia, and algae (i.e., ISO Test water, Elendt M4 medium, OECD TG 201 medium, AAP medium, and Bold's Basal Medium) in the presence and absence of Suwannee River Humic Acid (SRHA) as a function of time. Hydrodynamic size, particle sedimentation rate, and visual images of suspensions were analyzed for 96 h, and the SRHA concentration was varied from 0 to 10 mg/L. Zeta potential and water contact angle of CB-NP, and SRHA sorption to CB-NPs were also examined to complement stability analyses. CB-NPs always exhibited negative zeta potential regardless of media type and SRHA concentration, and became more negative in the presence of SRHA due to SRHA sorption. Moreover, CB-NPs were found to be hydrophobic in the absence of SRHA, whereas they became hydrophilic when SRHA was adsorbed. Stability test results showed that regardless of test media, the hydrodynamic size increased fast and the sedimentation rate was high in the absence of SRHA, indicating poor stability of the CB-NPs. Conversely, the presence of SRHA substantially increased the stability of CB-NPs over 96 h, regardless of the SRHA concentration and test media type. Stability trends in the presence and absence of SRHA were not consistent with predictions from classical Derjaguin–Landau–Verwey–Overbeek (DLVO) theory. However, extended and modified DLVO theories, that also accounted for hydrophobic-attractive forces due to the inherent nature of CB-NPs and steric repulsive forces associated with the brush-like

* Corresponding author at: Department of Mineral Resources and Energy Engineering, Chonbuk National University, Jeonju, Jeonbuk 54896, Republic of Korea.
E-mail address: kshjkim@jbnu.ac.kr (H. Kim).

https://doi.org/10.1016/j.colsurfa.2018.06.049
Received 15 March 2018; Received in revised form 7 June 2018; Accepted 18 June 2018
Available online 19 June 2018

conformation of SRHA adsorbed to CB-NPs, better described CB-NPs' stability in the absence and presence of SRHA, respectively.

1. Introduction

Engineered nanoparticles (ENPs) have drawn great attention in various industries and research fields owing to their small particle size (i.e., ≤ 100 nm in at least one characteristic dimension) and high surface-to-volume ratio, which result in unique physicochemical properties [1,2]. For example, carbon black nanoparticles (CB-NPs) are widely used in various products such as printing inks, paint, rubber, and coatings [1,3,4], and their global demand is expected to increase significantly [5]. The high and increasing production rate of CB-NPs implies an increase in the probability of exposure to the environment and living organisms, therefore calling for the need of risk assessment.

It is often reported that CB-NPs are toxic to aquatic organisms such as algae and daphnia [6,7]. Toxicity levels of NPs to living organisms vary depending on the NPs' dispersion status [8–10]. For instance, Zook et al. [8] observed significantly elevated hemolytic toxicity when silver nanoparticles were less aggregated. Sager et al. [9] indicated that the extent of toxicity of CB-NPs changes with their dispersion status; e.g., well-dispersed CB-NPs were almost 1.7 times more toxic than poorly dispersed ones. Ecotoxicity tests require a test medium appropriate to a target living organism, and the solution chemistry (e.g., ionic strength and ionic species) of the different test media varies widely [11–13]. It is therefore reasonable to expect that the dispersion status of NPs varies depending on the type of ecotoxicity medium. Furthermore, maintaining a well-dispersed status of hydrophobic CB-NPs in aqueous solution is not as simple as that of hydrophilic NPs [14,15]. Li et al. [14] observed that the dispersion stability of polyvinyl alcohol-encapsulated CB-NPs was improved in deionized water as compared with uncoated ones. Another study also recently reported that CB-NPs suspended in aqueous solution were extremely unstable in the absence of a dispersing agent, resulting in fast aggregation and sedimentation of CB-NPs [15]. Consequently, it is important to accurately understand the dispersion characteristics of toxic CB-NPs as a function of toxicity test media. However, very few studies have addressed this issue.

Humic acid is a representative natural organic matter that is ubiquitous in the aqueous environment, and it is known to be easily adsorbed to the surface of NPs and enhance their stability [15–19]. For instance, Hyung and Kim [16] observed enhanced stability of multi-walled carbon nanotubes in Milli-Q water in the presence of Suwannee River Humic Acid (SRHA). Han et al. [15] also observed a high stability of carboxyl-functionalized CB-NPs suspensions in the presence of SRHA that was not sensitive to the solution ionic strength or to the ion valence. Such high stability of NPs in the presence of SRHA is commonly attributed to a repulsive force, known as the steric force, acting between SRHA-adsorbed NPs [15,17]. Indeed, the National Institute of Standards and Technology developed and reported a protocol for preparing stable TiO_2-NPs suspensions in test media using SRHA. Toxicological assessments which employ stable NP suspensions reduce the complexity of data analysis and, accordingly, increase the reliability of toxicity data by eliminating the uncertainty in the particle size (distribution) [20]. Although the importance of obtaining information on the underlying mechanisms of NP stability in various toxicity media has gradually been acknowledged, relevant studies on toxic CB-NPs are very scarce. To the best of our knowledge, only a recent study investigated the stability of CB-NPs in an animal cell culture medium (i.e., Dulbeco's Modified Eagle's Media containing fetal bovine serum) using bovine serum albumin (BSA) as a dispersing agent [21]. The underlying mechanisms of NP stability were assessed using classical Derjaguin–Landau–Verwey–Overbeek (DLVO) theory, which predicts the interaction force between NPs by considering van der Waals and electrical double layer forces. However, this study did not fully unravel the exact dispersing mechanism in the presence of BSA, since it neglected non-DLVO forces such as hydrophobic and steric forces that are related to the intrinsic hydrophobic property of CB-NPs and the steric hindrance of adsorbed BSA molecules, respectively. In the present study, we will provide information on the dispersion characteristics of CB-NPs in ecotoxicity test media, along with an accurate mechanistic interpretation that may be useful for controlling the stability of CB-NP suspensions during toxicity tests.

The purpose of this study is to investigate the dispersion characteristics of CB-NPs suspended in ecotoxicity test media for various organisms in the absence and presence of SRHA. To examine the stability of CB-NPs in each test medium the sedimentation rate was assessed using a UV–Vis spectrophotometer. Furthermore, particles size changes were measured via the dynamic light scattering (DLS) method to evaluate their aggregation characteristics. To interpret the mechanism of interaction between CB-NPs, interaction energies were calculated using classical DLVO, extended DLVO (XDLVO), and modified DLVO (MDLVO) theories [17,22,23]. Classical DLVO, which considers electrostatic and van der Waals interactions, was found to provide an inadequate description of CB-NP stability in all cases. An improved interpretation of the stability of CB-NPs in absence and presence of SRHA was achieved using XDLVO and MDLVO theories which also accounted for hydrophobic and steric forces, respectively.

2. Materials and methods

2.1. CB-NPs and SRHA stock suspension preparation

Carbon black nanoparticles (CB-NPs; purity > 99%), which are a common ingredient of printing toner ink, were obtained from Birla carbon (South Korea); based on the manufacturer's report, this model has the highest production rate among all types in South Korea. The CB-NPs had spherical shape and a primary size of 25.7 ± 5.2 nm as measured using HR-TEM (JEM-2010, JEOL Ltd, Japan; Fig. 1). A 20 mg/L CB-NPs stock suspension was prepared in Milli-Q water (Millipore, Billerica, MA), and then dispersed in a sonication bath (Powersonic 420, Hwashin technology Co., South Korea) for 30 min. This stock suspension was diluted to the desired concentration for use in subsequent characterization and stability tests.

The stability of CB-NPs in ecotoxicity test media was investigated at various SRHA (Cat #2S101H, Standard II, International Humic Substances Society, USA) concentrations. SRHA stock solution was prepared following a procedure in the literature [17,24]. Briefly, 25 mg SRHA powder was dissolved in 50 mL sterilized Milli-Q water and stirred for 24 h. The solution was then filtered through 0.22-μm cellulose acetate membranes (Advantec, Tokyo, Japan). The pH of the filtrate was adjusted to 8.0 by adding 0.1 M NaOH, and then this solution was used as the stock solution. The total organic carbon (TOC) content of the SRHA stock solution was found to be 220 mg/L using a TOC analyzer (TOC-VCPH, Shimadzu Co., Japan). The SRHA stock solution was stored in the dark at 4 °C until use. SRHA solution with the desired concentration for all tests was prepared by diluting the stock solution.

2.2. Selection and preparation of ecotoxicity media

Five types of ecotoxicity media were selected for CB-NPs stability tests, including: ISO (International Organization for Standardization) Test water, Elendt M4 medium, OECD (Organization for Economic Cooperation and Development) TG 201 medium (ISO 8692), AAP (Algal

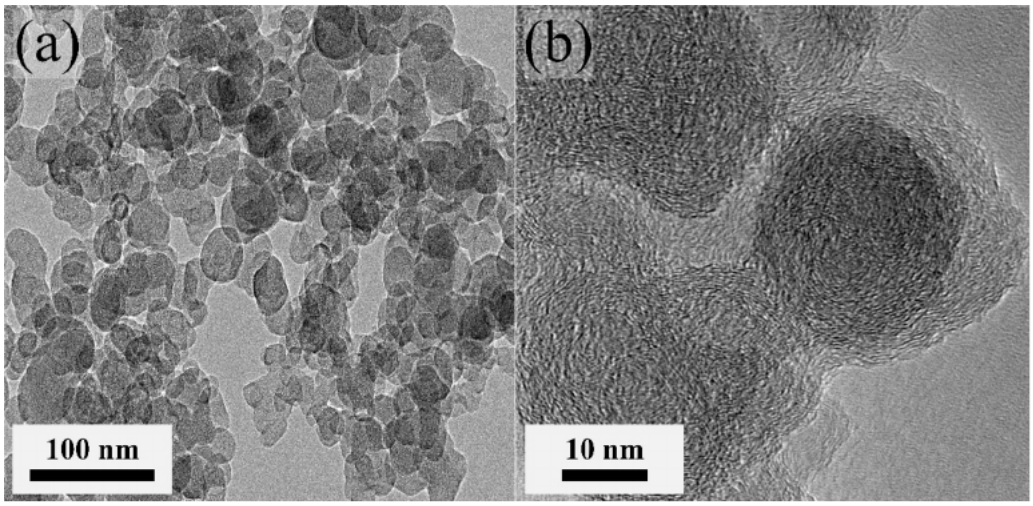

Fig. 1. (a) TEM image and (b) magnified TEM image of carbon black nanoparticles.

Assay Procedure) medium (US. EPA, ASTM), and Bold's Basal Medium (BBM). These media are commonly used for toxicity tests with fish [25], daphnia [26], and algae [27–29] cultures. Each medium was prepared based on the most commonly used guidelines [25–29]. The ionic composition, the measured pH, and the calculated ionic strength for test media are presented in Table S1.

2.3. Characterization of CB-NPs

The electrophoretic mobility of CB-NPs suspended in each ecotoxicity medium in the absence or presence of SRHA was measured using a zeta potential analyzer (ELS-Z, Otsuka Electronics Co., Japan). SRHA concentrations of 1, 5, and 10 mg/L were employed. The maximum threshold of 10 mg/L SRHA was selected based on previous research [30]. The measured electrophoretic mobility was converted to a zeta potential using the Smoluchowski equation [31]. The zeta potential of CB-NPs in the absence and presence of SRHA in the various ecotoxicity media is presented in Table 1.

The hydrophobic property of CB-NPs and their surface free energy components (γ_C^{LW}, γ_C^+, and γ_C^-; further described in detail in Section 2.6) were determined from contact angles measured using the captive bubble method [32–34] with a goniometer (DSA100 KRUSS, Hamburg, Germany). A conventional sessile drop method [35,36] was not employed in this study to minimize any errors caused by air capture in a capillary during measurement. The contact angles were measured on a CB-NPs lawn that was prepared by following a published procedure [37]. In brief, the CB-NPs' lawn was prepared by filtering the CB-NPs suspended in a desired toxicity medium with or without SRHA with a 0.22-μm–pore size cellulose acetate membrane filter under vacuum. After filtering, the CB-NPs layer (thickness = ~0.2 cm) was cut from the filters and fixed onto sample disks with double-sided adhesive tape. The CB-NPs layer was dried in a desiccator for 3 h, and then the layer was immersed and equilibrated in water. The captive bubble contact angle was measured, at least in triplicate, by observing the air bubble in water at room temperature.

2.4. CB-NPs stability tests in ecotoxicity media

Two types of experiments were carried out over 96 h to evaluate the stability of CB-NPs in each ecotoxicity medium, namely: sedimentation analysis and measurement of the hydrodynamic diameter. It is worthwhile mentioning that we set 96 h as the maximum test time, as it covers the time required for the short-term toxicity tests of fish, daphnia, and algae [25,26,29]. To prepare the sample suspensions for these stability tests, 100 mL of ecotoxicity media (four times concentrated), 100 mL Milli-Q water or SRHA solution (four times concentrated to a desired SRHA concentration), and 200 mL CB-NP suspension (two times concentrated in Milli-Q water) were prepared separately, and then mixed in a 500-mL beaker to prepare 400 mL sample with the desired concentration of CB-NPs (10 mg/L), SRHA (1, 5, and 10 mg/L), and other ions (see Table S1). This mixture was then placed in a sonication bath (Powersonic 420, Hwashin technology Co., South Korea) for 1 min to homogenize the suspension, and an aliquot of the sample was placed in a cuvette at room temperature (~25 °C) for 96 h to monitor the sedimentation behavior every 24 h [25,26,29]. The sedimentation behavior of CB-NPs in each test medium was assessed by measuring the absorbance at a wavelength of 600 nm using a UV–Vis spectrophotometer (HS-3300, Humas, South Korea). This wavelength was determined to minimize the interference of SRHA absorbance (Fig. S1). The absorbance reading was repeated three times for each sample, and the average value was reported. All tests were carried out at least in triplicate in order to increase data reliability. To support this sedimentation test visually, the 400-mL CB-NP suspension was also photographed every 24 h.

In addition to the sedimentation tests, the intensity-d_{50} hydrodynamic diameter of CB-NPs in suspension with or without SRHA was measured over 96 h via the DLS method (ELS-Z, Otsuka Electronics Co., Japan). The reflective index used for this measurement was 1.33. The sample suspension was prepared using the same procedure as for the sedimentation test. An aliquot (~2 mL) of the suspension was gently taken and placed in a disposable cuvette, and the hydrodynamic diameter was recorded every 24 h for 96 h. The stability tests and measurement readings were repeated at least three times under the same conditions.

Table 1
Zeta potential (mV) of CB-NPs suspended in five ecotoxicity media (ISO, M4, OECD, AAP, and BBM) in the absence and presence of SRHA. Three SRHA concentrations (1, 5, and 10 mg L^{-1}) were used. The replicate mean and standard deviation are presented (n = 10–15).

Medium	SRHA Concentration (mg/L)			
	w/o SRHA	1 mg/L SRHA	5 mg/L SRHA	10 mg/L SRHA
ISO	−10.4 ± 0.8	−13.4 ± 1.0	−13.4 ± 0.8	−14.0 ± 1.0
M4	−19.1 ± 1.6	−20.8 ± 1.2	−22.8 ± 1.4	−21.9 ± 1.0
OECD	−7.5 ± 0.9	−15.0 ± 0.8	−15.8 ± 0.7	−17.2 ± 0.1
AAP	−18.1 ± 1.2	−24.4 ± 0.2	−24.3 ± 1.9	−23.0 ± 1.9
BBM	−24.8 ± 1.2	−28.5 ± 0.3	−27.9 ± 0.6	−25.8 ± 0.2

2.5. SRHA adsorption test

The amount of SRHA adsorbed to CB-NPs was determined in each ecotoxicity medium with different SRHA concentrations using a batch equilibrium technique at room temperature. The sample preparation for this test follows the procedure described in the stability test (see Section 2.4). The initial SRHA concentrations in the glass vials were 1, 5, and 10 mg/L. The CB-NPs mass concentration added in each glass vial was 10 mg/L. The mixture volume for the adsorption tests was kept at 40 mL. The adsorption tests were carried out using a shaker (SIF-5000R, Lab companion, South Korea) at 100 rpm and 25 °C for 24 h. Note that adsorption equilibrium was reached within 24 h [38]. The CB-NPs suspension was then filtered using a 0.02-μm syringe filter (Anotop10, Whatman, USA) to separate the non-adsorbed SRHA from the mixture, and the SRHA concentration in the filtrate was measured [15,39]. Note that this separation method proved effective for separating non-adsorbed SRHA from CB-NPs (Table S2). The SRHA concentration was determined from the calibration curve of absorbance versus concentration (Fig. S2) using the UV–Vis Spectrophotometer at a wavelength of 254 nm. It should be noted that separate calibration curves were derived for each ecotoxicity medium. The amount of SRHA adsorbed to the unit mass of CB-NPs (Q_e, mg-SRHA/g-NPs) was determined as $(C_i\text{-}C_f)V/M_{NP}$ [40]; where V is the volume of suspension, M_{NP} is the mass of CB-NPs, and C_i and C_f are the SRHA concentration in bulk suspension at the initial and the equilibrium stage, respectively.

2.6. Interaction energy calculations

Total interaction energy profiles with separation distance between two interacting colloidal particles are frequently used in studies on the aggregation and dispersion of colloidal materials [31,41]. This information will enable us to interpret the interaction mechanism of experimentally observed stability and dispersion of CB-NPs in the different ecotoxicity media in the absence and presence of SRHA. Three different interaction energy calculations were considered, namely: classical DLVO, XDLVO, and MDLVO models. Each of these approaches will be briefly discussed below.

Classical DLVO theory is often used to calculate the interaction energy ($V_{classical}$ (h), Eq. (1)) between colloidal particles in an aqueous system as the sum of electrical double layer (Eq. (2)) and van der Waals (Eq. (3)) interactions as: [42,43]

$$V_{classical}(h) = V_{edl}(h) + V_{vdw}(h) \quad (1)$$

$$V_{edl}(h) = 32\pi\varepsilon_0\varepsilon_r a\left(\frac{k_B T}{ze}\right)^2 \Gamma^2 \exp(-\kappa h) \quad (2)$$

$$V_{vdw}(h) = -\frac{A_{CWC} a}{12h\left(1+\frac{14h}{\lambda}\right)} \quad (3)$$

where a represents the average radius of CB-NPs, ε_0 is the permittivity of vacuum, ε_r is the dielectric constant or the relative permittivity of water, k_B is the Boltzmann-constant, T is the absolute temperature, z is the valence of ions, e is the electron charge, Γ is the surface potential for the particle, κ is the inverse of the Debye length, h is the separation distance between two interacting NPs, λ is the dielectric wavelength that is usually taken as 100 nm [43], and A_{CWC} is the Hamaker constant for the CB-water-CB system.

Van Oss [44] presented a very simple method for the calculation of the Hamaker constant based on the surface energy of the material:

$$A_i = 24\pi d_0^2 \gamma_i^{LW} \quad (4)$$

where γ_i^{LW} is the Lifshitz–van der Waals apolar component of the surface energy of species i, and d_0 is the minimum equilibrium distance between the two interacting bodies, which has been found for a wide range of materials to be equal to 0.158 nm [45]. Values of γ_i^{LW} for CB-NPs shown in Table 2 were experimentally determined using the approach outlined in the next section. The combined Hamaker constant for the interaction between CB-NPs "C" in water "W" is given by:

$$A_{CWC} = \left(\sqrt{A_C} - \sqrt{A_W}\right)^2 \quad (5)$$

Through Eq. (4), the Hamaker constants of CB-NPs (A_C) in each test medium were determined (see the Table 2). These values were further used to calculate the value of A_{CWC} from Eq. (5) [44,46] and the Hamaker constant of water (A_W) equal to 3.70×10^{-20} J [47]. The calculated A_{CWC} are presented in Table 2.

Carbon-based nanomaterials (e.g., carbon nanotubes, fullerene, graphene, and carbon black) sometimes have hydrophobic properties in aqueous media [48]. Thus, a hydrophobic interaction (V_{hyd} (h)) between the CB-NPs cannot be ruled out. The total XDLVO interaction energy ($V_{extended}$ (h), Eq. (6) can be calculated by adding the hydrophobic interaction (Eq. (7)) into the classical DLVO interaction:

$$V_{extended}(h) = V_{edl}(h) + V_{vdw}(h) + V_{hyd}(h) \quad (6)$$

$$V_{hyd}(h) = 2\pi a \lambda_{AB} \Delta\Phi_{d_0}^{AB} \exp\left(\frac{d_0 - h}{\lambda_{AB}}\right) \quad (7)$$

where λ_{AB} is the water decay length for acid-base interaction and $\Delta\Phi_{d_0}^{AB}$

Table 2
Values of static contact angle (θ) and surface energy (γ) of CB-NPs, Hamaker constant of CB-NPs (A_C), and total Hamaker constant (A_{CWC}) for five ecotoxicity media in the absence and presence (1 mg L^{-1}) of SRHA.

Medium		Contact angle (°)			Surface energy (mJ/m²)[d]			A_C (J)[e]	A_{CWC} (J)[f]
		θ_W[a]	θ_F[b]	θ_B[c]	γ^{LW}	γ^+	$\gamma-$		
ISO	w/o SRHA	146	77	17	42.48	0.18	27.29	7.99×10^{-23}	3.36×10^{-20}
M4		138	65	25	40.33	2.56	31.62	7.59×10^{-23}	3.37×10^{-20}
OECD		129	60	20	41.76	2.88	25.03	7.86×10^{-23}	3.36×10^{-20}
AAP		126	62	19	42.01	1.96	19.55	7.90×10^{-23}	3.36×10^{-20}
BBM		144	74	23	40.94	0.66	28.65	7.70×10^{-23}	3.37×10^{-20}
ISO	1 mg/L SRHA	83	11	45	32.34	13.66	0.75	6.08×10^{-23}	3.40×10^{-20}
M4		68	10	25	40.33	6.08	2.46	7.59×10^{-23}	3.37×10^{-20}
OECD		62	21	41	34.17	6.01	7.47	6.43×10^{-23}	3.39×10^{-20}
AAP		64	12	31	38.28	5.99	4.83	7.20×10^{-23}	3.38×10^{-20}
BBM		66	11	47	31.40	9.81	3.35	5.91×10^{-23}	3.41×10^{-20}

[a] average value of contact angle of CB-NPs in water measured by a captive bubble method (n ≥ 3) [32].
[b] average value of contact angle of CB-NPs in Formamide measured by a captive bubble method (n ≥ 3) [32].
[c] average value of contact angle of CB-NPs in 1-bromonaphthalene measured by a captive bubble method (n ≥ 3) [32].
[d] adopted from van Oss [44].
[e] determined with Eq. (4).
[f] determined with Eq. (5). For this calculation, 3.70×10^{-20} J was used as water Hamaker constant [47].

is the free energy of attachment at d_0. The value of $\Delta\Phi_{d_0}^{AB}$ can be determined using the following equations: [44,46]

$$\Delta\Phi_{d_0}^{AB} = 2[\sqrt{\gamma_L^+}(\sqrt{\gamma_C^-} + \sqrt{\gamma_C^-} - \sqrt{\gamma_L^-}) + \sqrt{\gamma_L^-}(\sqrt{\gamma_C^+} + \sqrt{\gamma_C^+} - \sqrt{\gamma_L^+}) - \sqrt{\gamma_C^+\gamma_C^-} - \sqrt{\gamma_C^-\gamma_C^+}] \quad (8)$$

$$(1+\cos\theta)\,\gamma_L = 2(\sqrt{\gamma_C^{LW}\gamma_L^{LW}} + \sqrt{\gamma_C^+\gamma_L^-} + \sqrt{\gamma_C^-\gamma_L^+}) \quad (9)$$

where θ is the contact angle of CB-NPs that was determined by the bubble captive method [49], γ is the surface energy, and subscripts "*L*" and "*C*" indicate the liquid and CB−NPs, respectively, and superscripts "+," and "−" denote the electron acceptor and the donor parameter, respectively. Contact angles between the CB-NPs surface and three different liquids (water, formamide, and 1-Bromonaphthalene) were measured to calculate unknown surface energies of CB-NPs (γ_C^{LW}, γ_C^+ and γ_C^-) using the Young-Dupré equation (Eq. (9) [44,46]. Other surface free energies in Eq. (9) were taken as: $\gamma_L^{LW} = 21.8\,mJ/m^2$, $\gamma_L^+ = 25.5\,mJ/m^2$, $\gamma_L^- = 25.5\,mJ/m^2$ for water (polar); $\gamma_L^{LW} = 39\,mJ/m^2$, $\gamma_L^+ = 2.28\,mJ/m^2$, $\gamma_L^- = 39.6\,mJ/m^2$ for formamide (polar); and $\gamma_L^{LW} = 44.4\,mJ/m^2$, $\gamma_L^+ = 0\,mJ/m^2$, $\gamma_L^- = 0\,mJ/m^2$ for 1-Bromonaphthalene (apolar). The measured contact angle and the corresponding calculated surface free energies of the CB-NPs are shown in Table 2.

Numerous studies have reported experimental deviations from classical DLVO predictions in the presence of SRHA [17]. The steric force (F_{str} (*h*), Eq. (12) has been proposed to explain these deviations when two particles with brush layers interact [42]. The MDLVO interaction energy prediction ($V_{modified}$ (*h*), Eq. (10) includes terms for this steric interaction (V_{str} (*h*), Eq. (11) in the presence of SRHA as:

$$V_{modified}(h) = V_{edl}(h) + V_{vdw}(h) + V_{str}(h) \quad (10)$$

$$V_{str}(h) = -\int_{\infty}^{h} F_{str}(h)dh \text{ for } h < 2L \quad (11)$$

$$F_{str}(h) = \pi a\left(\frac{k_B T}{s^3}\right)\left\{\frac{8l}{5}\left[\left(\frac{2l}{h}\right)^{5/4} - 1\right] + \frac{8l}{7}\left[\left(\frac{h}{2l}\right)^{7/4} - 1\right]\right\} \quad (12)$$

$$s = \sqrt{\frac{M}{N \times Q_i}} \quad (13)$$

where V_{str} (*h*) is the steric interaction energy, *s* is the distance between SRHA chains adsorbed on a CB-NP's surface which was determined with Eq. (13) [50], *M* represents the molecular weight of SRHA (1490 g/mole [51] in the present study), *N* is Avogadro's number ($6.02 \times 10^{23} mol^{-1}$), Q_i is the adsorption amount of SRHA on a CB-NP's surface in each test medium (mg/m^2), and *l* is the brush thickness (assumed to be 2.5 nm) [17].

3. Results

3.1. Electrokinetic and hydrophobic properties of CB-NPs

Table 1 presents the zeta potential of CB-NPs suspended in five ecotoxicity media when the SRHA concentration was 0, 1, 5, and 10 mg/L. The CB-NPs were always negatively charged, but tended to be slightly more negative in the presence of SRHA. The zeta potential of other NPs has similarly been reported to be more negative in the presence of SRHA because of the adsorption of negatively charged SRHA [17,18,52–54]. Zeta potential is known to be sensitive to and correlated with solution chemistry (e.g., ionic strength, pH, ion valence) [55]. However, no correlation could be established between the zeta potential of CB-NPs with either the ionic strength or pH of the different media. This result can likely be attributed to adsorption of hydrated cations/anions in the media (Table S1) on the surface of CB-NPs.

The surface hydrophobicity of CB-NPs suspended in different ecotoxicity media without and with SRHA was evaluated by measuring their contact angles in the presence of air and water (θ_W). Measured values of θ_W are presented in Table 2. The average contact angles of CB-NPs in the absence of SRHA were always greater than 120° for all test media, indicating that the surface is hydrophobic. Conversely, the surface of CB-NPs was hydrophilic in the presence of SRHA ($\theta_W < 83°$).

3.2. Stability of CB-NPs in the absence of SRHA

Colloidal stability of CB-NPs suspended in ecotoxicity media in the absence of SRHA was first assessed by measuring the change of hydrodynamic diameter over time. Fig. 2 and Table S3 show the change in the size of CB-NPs in each test medium over 96 h. The initial size of CB-NPs (i.e., at < 10 min after sample preparation) suspended in different media ranged from 186 to 2189 nm. The initial hydrodynamic size of CB-NPs in monovalent salt with low ionic strength (1 mM) was much larger (~200 nm) than their primary size (~27 nm). This observation suggests that incomplete dispersion and/or fast aggregation can explain the initial size of CB-NPs in the test media. After 24 h, the hydrodynamic diameter of CB-NPs increased regardless of the type of test media and ranged from 312 to 6089 nm, further confirming severe aggregation of CB-NPs with time. This observation indicates that aggregation of CB-NPs easily occurred in the various test media in the absence of SRHA. Hydrodynamic diameters greater than 7.0 μm could not be accurately measured with our equipment because of the instrument detection limit. Consequently, the CB-NPs size after 24 h was not presented in Fig. 2 for some of the test media. No reliable CB-NP hydrodynamic diameter could be obtained after 48 h because the size of CB-NPs in all the media was greater than 7.0 μm.

In addition to hydrodynamic diameter measurements shown in Fig. 2, the stability of CB-NPs was also assessed by measuring the sedimentation behavior of CB-NPs in the five different test media in the absence of SRHA. Fig. 3 presents the measured relative absorbance value versus lapsed time in these experiments. Sedimentation results reveal that CB-NPs are not stable during the 96 h test period in all media without SRHA. The settling rate of CB-NPs in the OECD medium was slower than that in other media, with about 82% CB-NPs settled after 96 h. For all other test media, about 70% to > 96% of the CB-NPs settled after 24 h and 96 h, respectively. The observed high CB-NPs settling rate in all test media is consistent with the variation of their hydrodynamic size shown in Fig. 2. Low stability has been similarly observed for oxide nanoparticles and bare carbon-based NPs [38,42,56].

Figure S4 shows photo images of the CB-NP suspensions in the five different test media over 96 h. The images clearly show settlement of CB-NPs over time, which supports the observed size growth (Fig. 2) and the low stability of CB-NPs (Fig. 3) in the examined test media.

3.3. Stability of CB-NPs in the presence of SRHA

Several studies have reported that the presence of humic acid can enhance the stability of NP suspensions [16,17,39]. Enhanced NP stability can make the NP toxicity test much easier and increase the data reliability by eliminating the size heterogeneity in the system. In fact, inclusion of humic acid in the toxicity assay of titanium dioxide NPs has been reported as a standard protocol [30]. We therefore also investigated the role of SHRA in the stability of CB-NP suspensions. Stability tests were conducted at SRHA concentration levels of 1, 5, and 10 mg/L.

The hydrodynamic diameter and sedimentation behavior of CB-NPs in the five test media in the presence of SRHA is shown in Figs. 2 and 3, respectively. The initial hydrodynamic diameter of CB-NPs ranged from 115 to 154 nm depending on test media in the presence of SRHA. After 96 h, the hydrodynamic diameter of CB-NPs was very similar to the initial value when the SRHA concentration ranged from 1 to 10 mg/L. For example, the hydrodynamic diameter ranged from 141 to 266 nm in all test media when the SRHA was equal to 1 mg/L. Here, it should be

noted that the sizes reported in Fig. 2 are almost identical with those measured at much earlier time scale (0–64 min) (Fig. S3). These observations indicate that little CB-NP aggregation occurred in the presence of SRHA, even when SRHA was 1 mg/L. Sedimentation tests were carried out for 96 h. The sedimentation rate was very low in the presence of SRHA and tended to decrease slightly with further increases in SRHA concentration (Fig. 3). The low sedimentation rate of CB-NP in the presence of SRHA is consistent with the nearly constant hydrodynamic diameter over the test period (Fig. 2). Close inspection of this data reveals that the settling rate of CB-NPs suspended in ISO and BBM media with 1 mg/L SRHA appears to be slightly greater than those in other media. However, no difference in settling with media type was observed at 5 and 10 mg/L SRHA.

In comparison to stability experiments in the absence of SRHA (Section 3.2), CB-NP suspensions in all test media with SRHA had much lower hydrodynamic diameters and settling rates, and this reflects much greater CB-NP stability. Similarly, photo images of CB-NP suspensions in the test media in the presence of SRHA over 96 h also showed almost no visible change in the suspension properties (Fig. S4), while significant aggregation and settling of CB-NPs was observed in the absence of SRHA.

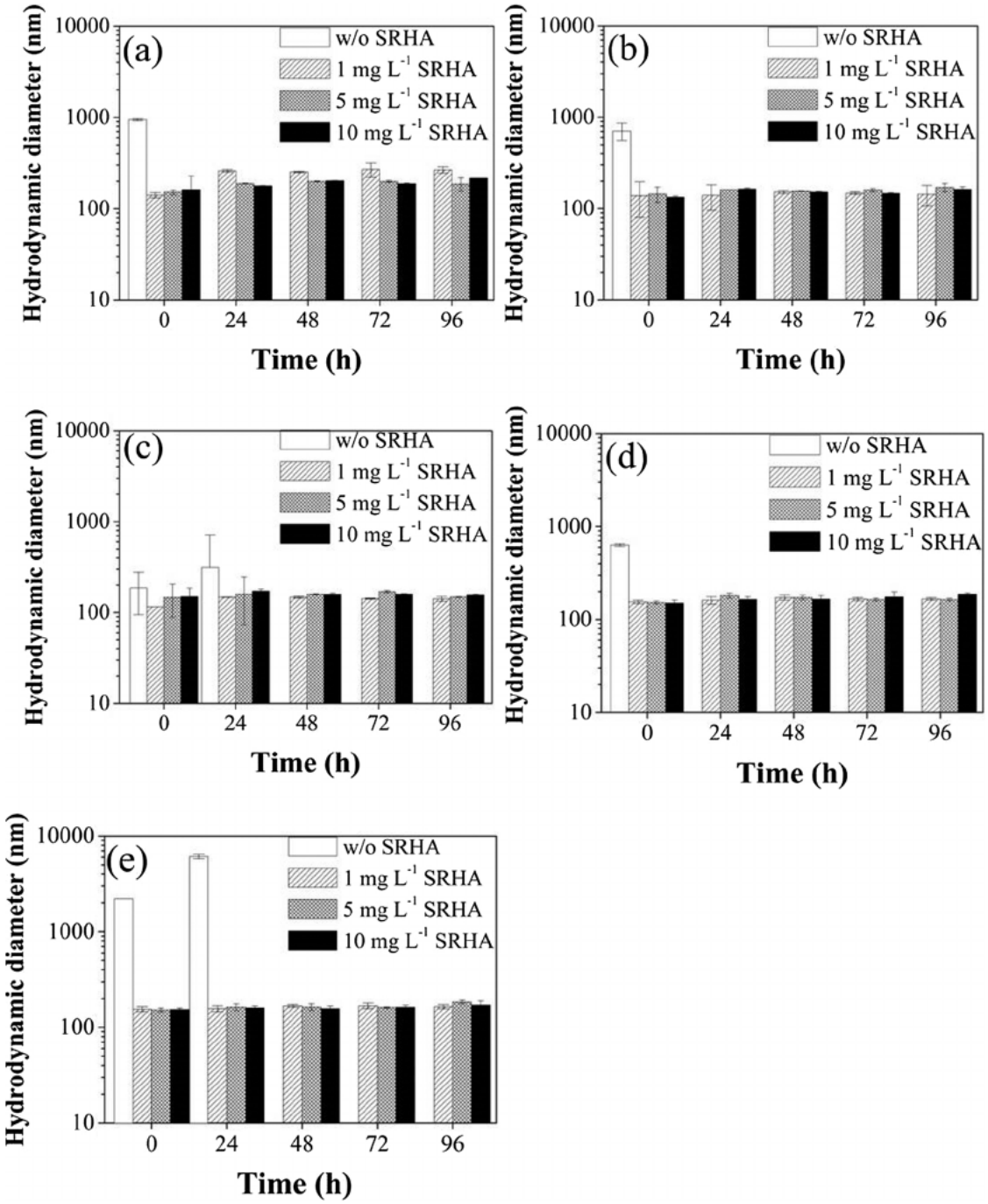

Fig. 2. Change of the hydrodynamic diameter of CB-NPs over time. The CB-NPs were suspended in (a) ISO, (b) M4, (c) OECD, (d) AAP, and (e) BBM medium in the absence and presence of SRHA. The final concentration of NP suspension for all tests was 10 mg L^{-1}. Three SRHA concentrations (1, 5, and 10 mg L^{-1}) were used. Note that 0 h represents the result measured within 10 min upon completion of sample preparation. The maximum size threshold of the equipment was exceeded in media without SRHA after 24 or 48 h, and in this case no results are reported. Error bars represent standard deviations from replicate experiments ($n \geq 3$).

4. Discussion

4.1. Interaction mechanism of CB-NPs in the absence of SRHA: hydrophobic effect

To interpret the CB-NPs stability mechanism, the total interaction energy profile between CB-NPs in each medium was calculated based on classical DLVO theory, and the results are presented in Fig. 4 and Table S4. DLVO interaction energy profiles predict no energy barrier between CB-NPs in the ISO, M4, and OECD culture media. In this case, attractive interactions between CB-NPs (e.g., favorable conditions) can explain the rapid growth of the CB-NP size and suspension instability (Figs. 2, 3, and S4). However, deviations from DLVO theory were observed for CB-NPs in AAP and BBM media. In particular, energy barriers of ~24 and ~36 kT (e.g., unfavorable conditions) were predicted between CB-NPs in AAP and BBM media, respectively. Other than diffusion, no external forces were applied in the static systems employed to measure the hydrodynamic diameter and sedimentation behavior. The kinetic energy of diffusing NPs can only overcome the energy barrier of a few kT [41]. Consequently, these energy barriers are predicted to be sufficiently large to maintain the stability of the CB-NP suspension. In contrast to these DLVO predictions, fast aggregation and settling rates of CB-NPs were observed in the AAP and BBM media. Many previous studies on NP aggregation have reported similar deviations from

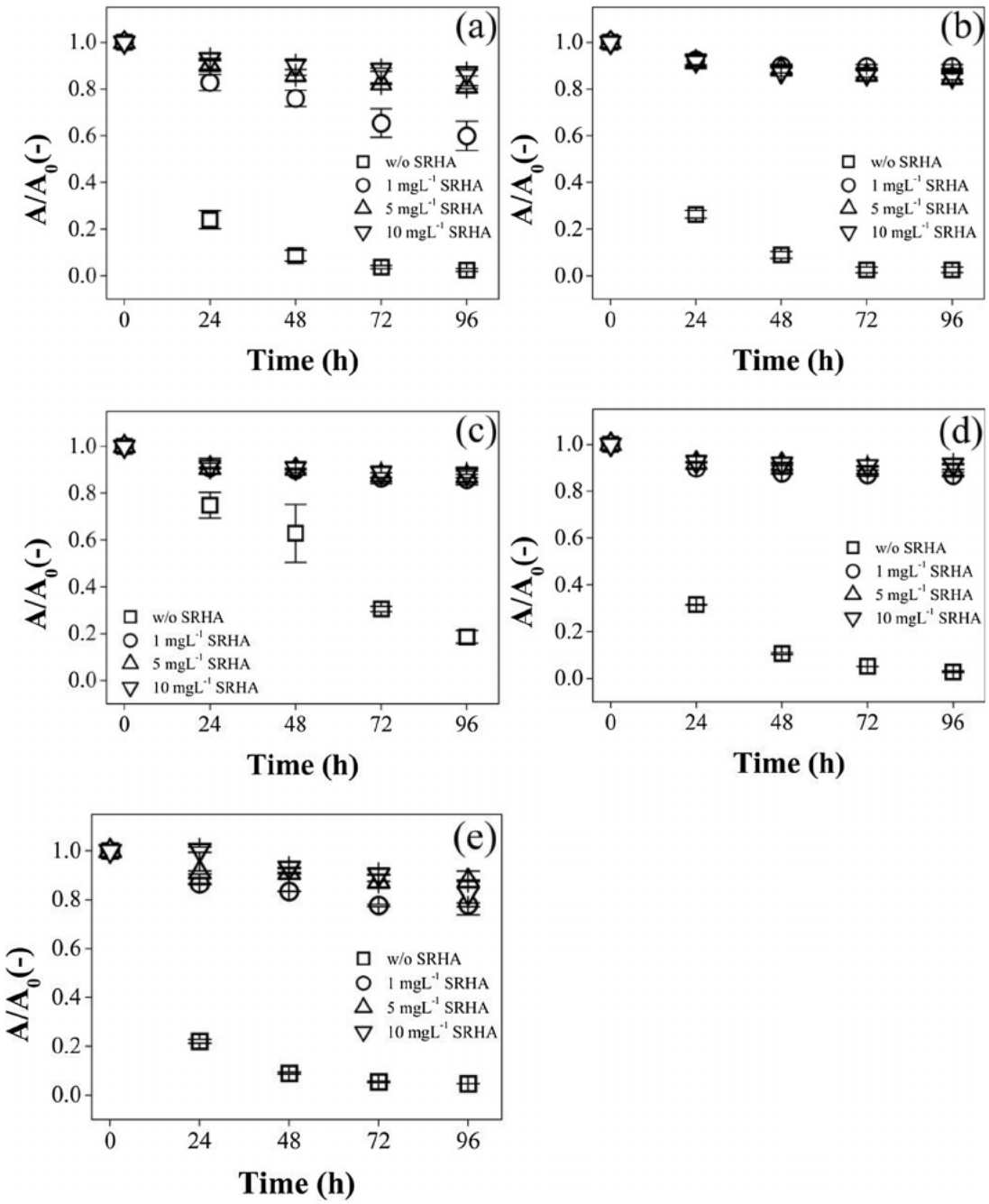

Fig. 3. Change of the normalized concentration (A/A_0) of CB-NP suspension over time. The CB-NPs were suspended in (a) ISO, (b) M4, (c) OECD, (d) AAP, and (e) BBM medium in the absence and presence of SRHA. The final concentration of NP suspension for all tests was 10 mg L^{-1}. Three SRHA concentrations (1, 5, and 10 mg L^{-1}) were used. A and A_0 represent the absorbance values of NP suspension measured at an arbitrary time t and 0 h, respectively. Note that 0 h represents the result measured within 10 min upon completion of sample preparation. Error bars represent standard deviations from replicate experiments ($n \geq 3$).

classical DLVO predictions [15,22,57–59]. The above observations clearly support that additional forces were likely involved in the stability mechanism of CB-NPs in the absence of SRHA.

The CB-NPs used in the present study were found to be hydrophobic based on the measured contact angle values in the five test media (≥126°) (Table 2). Previous studies have also reported that carbon-based particles are hydrophobic due to their low surface free energy [60,61]. In this case, surface interaction is governed by DLVO forces (electrostatics and van der Waals) and a long-ranged hydrophobic force [62,63]. Hence, XDLVO theory that accounts for these forces was employed to better interpret the stability mechanism of CB-NPs in the absence of SRHA. The XDLVO interaction energy calculation results suggest no energy barrier in all media tested (Fig. 5a and Table S4), indicating favorable conditions for NP interaction. These XDLVO predictions are consistent with the hydrodynamic diameter and sedimentation analyses in Figs. 2 and 3, respectively, that show severe aggregation/sedimentation in all test media. In addition to electrostatic and van der Waals interactions, the observed severe aggregation and fast sedimentation of CB-NPs in the five test media can also be attributed to the hydrophobic nature of CB-NPs, which is an inherent property of carbon-based nanoparticles [21]. Meanwhile, a relatively slower settling rate was observed in the OECD medium than other test media (see and compare the data measured at 24 h in Fig. 3). This trend can be attributed to the fact that the separation distance where the attractive interaction between CB-NPs takes place is relatively shorter for the OECD medium than others (Fig. 5a). Previous studies have also reported the greater rate of particle deposition when the energy well forms at larger distance [64,65].

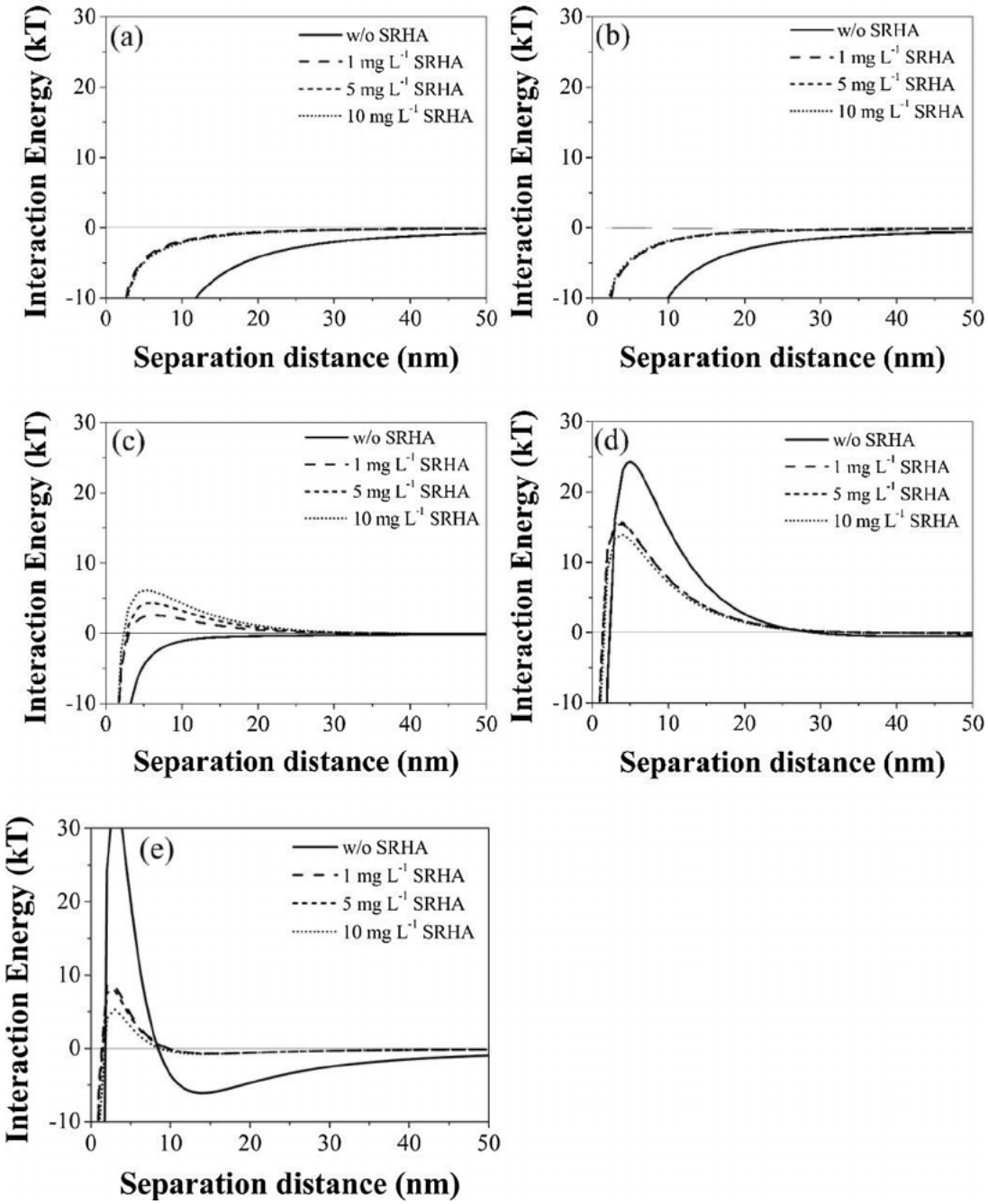

Fig. 4. The classical DLVO interaction energy profiles were calculated between CB-NPs with different five types of media (a) ISO, (b) M4, (c) OECD, (d) AAP, and (e) BBM in the absence and presence of SRHA (1, 5, and 10 mg L^{-1}) as a function of the separation distance.

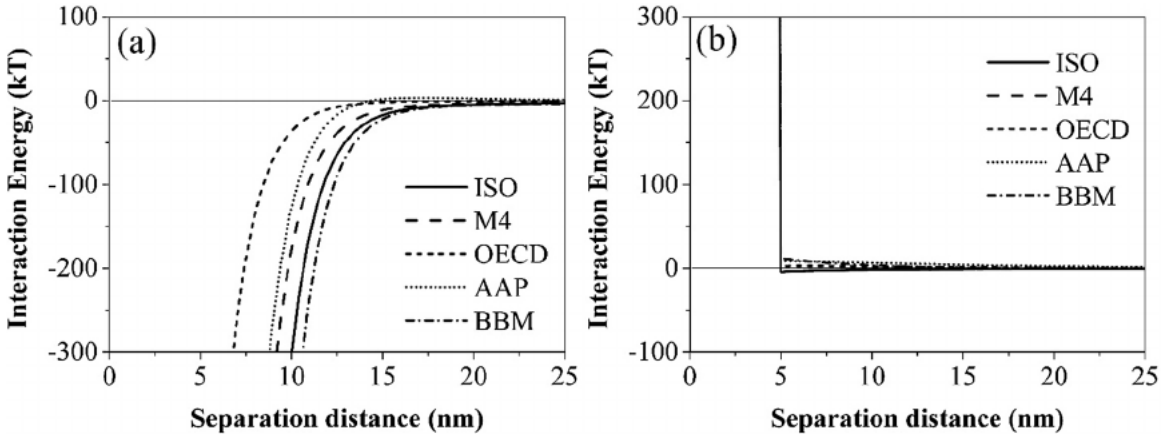

Fig. 5. Calculated (a) extended DLVO (XDLVO) and (b) modified DLVO (MDLVO) interaction energy profiles between CB-NPs suspended in five ecotoxicity media (ISO, M4, OECD, AAP, and BBM). The XDLVO interaction energy profiles were determined in the absence of SRHA. The MDLVO interaction energy profiles were obtained in the presence of 1 mg L^{-1} SRHA.

4.2. Interaction mechanism of CB-NPs in the presence of SRHA: steric effect

Results presented in Sections 3.2 and 3.3 (e.g., hydrodynamic diameters in Fig. 2 and Table S3, sedimentation behavior in Fig. 3, and photo images of suspensions over time in Fig. S4) clearly indicate that the presence of SRHA significantly improved the stability of CB-NPs suspended in all ecotoxicity media as compared to those without SRHA. Moreover, the enhanced stability of CB-NPs was observed for all of the considered SRHA concentrations, even when a low SRHA concentration of 1 mg/L was present.

Recall that classical DLVO theory could not explain the dispersion characteristics of the CB-NPs in the absence of SRHA (Section 4.1). Below we investigate the ability of DLVO theory to explain CB-NP stability in the presence of SRHA. DLVO interaction energy profiles are presented in Fig. 4, and the corresponding energy barriers are summarized in Table S4. DLVO calculations predict the absence of an energy barrier (e.g., favorable conditions) for the ISO and M4 media, but presence of an energy barrier (e.g., unfavorable conditions) for the remaining test media (i.e., OECD, AAP, and BBM). This trend is consistent with all of the tested SRHA concentrations. In addition, there is a small probability that CB-NPs can diffuse over the ~10 kT energy barrier in OECD and BBM media to aggregate [41]. This observation and DLVO interpretation leads us to deduce that the stability of CB-NPs would follow the following order: AAP > OECD ≅ BBM > ISO ≅ M4. However, these predictions are not consistent with the size (Fig. 2) and sedimentation results (Figs. 3 and S4). Consequently, classical DLVO theory is not sufficient for interpreting the stability of the CB-NPs suspension in the presence of SRHA.

XDLVO interactions (that included hydrophobic forces) provided an improved interpretation of CB-NP stability behavior in the absence of SRHA (Section 4.1). In this case, the surface of the CB-NP was hydrophobic (contact angle > 126° in Table 2). In contrast, Table 2 indicates that surface of the CB-NP was always hydrophilic in the presence of SRHA (contact angle < 83°). Furthermore, almost identical contact angles were observed between the CB-NPs suspended in culture media with 5 and 10 mg/L SRHA versus those with 1 mg/L SRHA. Similarly, Ramos-Tejada et al. [66] reported negligible change of contact angles of hematite over a wide range of SRHA concentration values (1 to 200 mg/L): 26 ± 1° and 25.3 ± 0.5° for 1 and 200 mg/L SRHA, and accordingly, similar values of hematite surface free energy. The static contact angles shown in Table 2 are known to be greater than the receding contact angle [67]. Law [68] proposed that the hydrophobicity of a solid surface can be determined from the receding contact angle, with the threshold value of 90°. Hence, we ruled out the effect of a hydrophobic force for the CB-NPs surface in the presence of SRHA. Here, it is worthwhile noting that a hydrophobic force is only one component of a Lewis acid-base interaction [69]; it also includes a hydration force when the solid surface is hydrophilic. One could argue on the consideration of the hydration force in the presence of SRHA; however, it has been widely accepted that the hydration force can take place when a solid surface is strongly hydrophilic (θ < 15°) [70,71]. The CB-NPs in the presence of SHRA was not strongly hydrophilic, suggesting that another component of the Lewis acid-base interaction can also be neglected. In fact, the calculated XDLVO interaction energies (including a hydration force) for the CB-NPs with 1 mg/L SHRA predict no energy barrier for all culture media (Figure S5), which cannot explain the observed stability results (Figs. 2, 3 and S4). Based on all described above, thus, we did not further discuss the XDLVO interaction.

When SRHA is adsorbed on a solid, it creates a brush-like surface that produces a steric hindrance force [15–17]. A steric force from adsorbed SRHA is normally repulsive [72], which reduces the aggregation of NPs and their sedimentation, and eventually increases the NP stability [73,74]. Eq. (12) was employed to determine the steric force between two brush-like particles. The corresponding MDLVO interaction energy profiles for CB-NPs in the five ecotoxicity media in the presence of 1 mg/L SRHA is shown in Fig. 5b. A sizable energy barrier (Φ_{max} > 300 kT) was observed for all test media in the presence of 1 mg/L SRHA after incorporating the steric force into the classical DLVO interaction (Table S4 and Fig. 5b). Note that the sizable energy barrier was observed with various brush layer thickness for all test media (Fig. S5), implying no change in our conclusion that the presence of SRHA increases the stability of CB-NPs in all test media. Meanwhile, higher SRHA concentrations lead to a much stronger repulsive steric force due to greater adsorption of SRHA to NPs (see Table S5), and were therefore not considered in MDLVO calculations. The CB-NPs cannot overcome such a huge energy barrier for aggregation, which is consistent to the observed enhanced stability of CB-NPs in the presence of SRHA (Figs. 2, 3, S4, and Table S3). Similarly, previous studies have reported improved stability of hydrophobic particles by SRHA in aqueous systems [72,75].

Although the MDLVO interaction energy prediction explains the greater stability of CB-NPs in the presence than absence of SRHA, a slightly higher sedimentation rate was observed in ISO and BBM media with 1 mg/L SRHA than in the other three media (i.e., M4, OECD, and AAP) (Fig. 3). This suggests slightly lower stability in ISO and BBM media than in the other test media. This observation is not consistent with the MDLVO interaction energy results since the predicted energy barrier is insurmountable for CB-NPs to overcome by diffusion. A plausible explanation for the enhanced stability of CB-NPs in the test media in the presence of SRHA is due to nanoscale roughness and/or

chemical heterogeneity which were neglected in our interaction energy calculations [76–79]. Indeed, nanoscale roughness has recently been demonstrated to provide a viable alternative explanation for enhanced stability behavior that has previously been attributed to electrosteric repulsion [76–78]. To systematically study the effects of roughness on interaction energies would require relating SRHA sorption results (Table S5) to nanoscale roughness parameter, which is beyond the scope of the present study.

5. Conclusions

Experimental studies and interaction energy calculations were conducted to investigate the stability mechanism of CB-NPs suspended in five different ecotoxicity test media in the presence and absence of SRHA. Fast aggregation-sedimentation was observed for CB-NPs in the absence of SRHA, whereas the CB-NPs suspensions were very stable during a 96 h test period in the presence of SRHA. This enhanced stability for CB-NPs occurred even in the presence of a low SRHA concentration of 1 mg/L, and was not influenced much by further increases in SRHA concentration up to 10 mg/L. The classical DLVO theory failed to predict the stability of CB-NPs both in the absence and presence of SRHA for all tested media. However, the stability of CB-NPs in the absence of SRHA was successfully predicted by XDLVO theory that considered a hydrophobic force that was related to measured contact angles and surface free energies of the CB-NP surface. In the presence of SRHA, a strong repulsive force was predicted from steric hindrance of brush-like layers of absorbed SRHA on CB-NPs. MDLVO theory that considered this steric force successfully predicted the stability of CB-NPs in test media with SRHA.

Findings from this study provide insights on the limitations of traditional approaches to predict the stability of CB-NPs in the absence and presence of SRHA. Furthermore, this study provides useful information on controlling the stability of CB-NPs suspension in ecotoxicity test media. This information will facilitate the design of reproducible toxicity tests by minimizing the complexity (e.g., time-dependent size variation) and uncertainty associated with unstable CB-NPs suspensions in ecotoxicity test media.

Acknowledgements

This research was supported by the National Institute of Environmental Research (NIER-SP2014-231), Ministry of Environment of Korea, the Basic Science Research Program through the National Research Foundation of Korea (NRF) funded by the Ministry of Education (NRF-2015R1D1A3A01020766), the research funds of Chonbuk National University in 2017, and the Korea Energy and Mineral Resources Engineering Program (KEMREP).

Appendix A. Supplementary data

Supplementary material related to this article can be found, in the online version, at doi:https://doi.org/10.1016/j.colsurfa.2018.06.049.

References

[1] C. Barrie, P. Griffiths, R. Abbott, I. Grillo, E. Kudryashov, C. Smyth, Rheology of aqueous carbon black dispersions, J. Colloid Interf. Sci. 272 (2004) 210–217.
[2] K.V. Hoecke, J.T. Quik, J. Mankiewicz-Boczek, K.A.D. Schamphelaere, A. Elsaesser, P.Vd. Meeren, C. Barnes, G. McKerr, C.V. Howard, D.V.D. Meent, Fate and effects of CeO_2 nanoparticles in aquatic ecotoxicity tests, Environ. Sci. Technol. 43 (2009) 4537–4546.
[3] S. Hussain, S. Boland, A. Baeza-Squiban, R. Hamel, L.C.J. Thomassen, J.A. Martens, M.A. Billon-Galland, J. Fleury-Feith, F. Moisan, J.C. Pairon, F. Marano, Oxidative stress and proinflammatory effects of carbon black and titanium dioxide nanoparticles: role of particle surface area and internalized amount, Toxicology 260 (2009) 142–149.
[4] J.K. Kang, I.G. Yi, J.A. Park, S.B. Kim, H. Kim, Y. Han, P.J. Kim, I.C. Eom, E. Jo, Transport of carboxyl-functionalized carbon black nanoparticles in saturated porous media: column experiments and model analyses, J. Contam. Hydrol. 177 (2015) 194–205.
[5] J. Lohwacharin, S. Takizawa, R. Punyapalakul, Carbon black retention in saturated natural soils: effects of flow conditions, soil surface roughness and soil organic matter, Environ. Pollut. 205 (2015) 131–138.
[6] L. Canesi, R. Fabbri, G. Gallo, D. Vallotto, A. Marcomini, G. Pojana, Biomarkers in Mytilus galloprovincialis exposed to suspensions of selected nanoparticles (nano carbon black, C_{60} fullerene, nano-TiO_2, nano-SiO_2), Aquat. Toxicol. 100 (2010) 168–177.
[7] H.D. Nielsen, L.S. Berry, V. Stone, T.R. Burridge, T.F. Fernandes, Interactions between carbon black nanoparticles and the brown algae Fucus serratus: inhibition of fertilization and zygotic development, Nanotoxicology 2 (2008) 88–97.
[8] J.M. Zook, R.I. MacCuspie, L.E. Locascio, M.D. Halter, J.T. Elliott, Stable nanoparticle aggregates/agglomerates of different sizes and the effect of their size on hemolytic cytotoxicity, Nanotoxicology 5 (2011) 517–530.
[9] T.M. Sager, D.W. Porter, V.A. Robinson, W.G. Lindsley, D.E. Schwegler-Berry, V. Castranova, Improved method to disperse nanoparticles for in vitro and in vivo investigation of toxicity, Nanotoxicology 1 (2007) 118–129.
[10] J. Gao, S. Youn, A. Hovsepyan, V.L. Llaneza, Y. Wang, G. Bitton, J.-C.J. Bonzongo, Dispersion and toxicity of selected manufactured nanomaterials in natural river water samples: effects of water chemical composition, Environ. Sci. Technol. 43 (2009) 3322–3328.
[11] L.A. Millington, K.H. Goulding, N. Adams, The influence of growth-medium composition on the toxicity of chemicals to algae, Water Res. 22 (1988) 1593–1597.
[12] A. Samel, M. Ziegenfuss, C. Goulden, S. Banks, K. Baer, Culturing and bioassay testing of Daphnia magna Using Elendt M4, Elendt M7, and COMBO media, Ecotox. Environ. Safety 43 (1999) 103–110.
[13] J. Seo, S. Kim, S. Choi, D. Kwon, T.-H. Yoon, W.-K. Kim, J.-W. Park, J. Jung, Effects of physiochemical properties of test media on nanoparticle toxicity to Daphnia magna straus, Bull. Environ. Contam. Toxicol. 93 (2014) 257–262.
[14] H.-Y. Li, H.-Z. Chen, W.-J. Xu, F. Yuan, J.-R. Wang, M. Wang, Polymer-encapsulated hydrophilic carbon black nanoparticles free from aggregation, Colloids Surf. A: Physicochem. Eng. Asp. 254 (2005) 173–178.
[15] Y. Han, G. Hwang, S. Park, A. Gomez-Flores, E. Jo, I.-C. Eom, M. Tong, H.-J. Kim, H. Kim, Stability of carboxyl-functionalized carbon black nanoparticles: the role of solution chemistry and humic acid, Environ. Sci.: Nano 4 (2017) 800–810.
[16] H. Hyung, J.-H. Kim, Natural organic matter (NOM) adsorption to multi-walled carbon nanotubes: effect of NOM characteristics and water quality parameters, Environ. Sci. Technol. 42 (2008) 4416–4421.
[17] X.J. Jiang, M.P. Tong, H. Kim, Influence of natural organic matter on the transport and deposition of zinc oxide nanoparticles in saturated porous media, J. Colloid Interf. Sci. 386 (2012) 34–43.
[18] P. Han, X. Wang, L. Cai, M. Tong, H. Kim, Transport and retention behaviors of titanium dioxide nanoparticles in iron oxide-coated quartz sand: effects of pH, ionic strength, and humic acid, Colloids Surf. A: Physicochem. Eng. Aspects 454 (2014) 119–127.
[19] H. Yang, H. Kim, M. Tong, Influence of humic acid on the transport behavior of bacteria in quartz sand, Colloids Surf. B 91 (2012) 122–129.
[20] J. Taurozzi, V. Hackley, M. Wiesner, Preparation of Nanoscale TiO_2 Dispersions in Biological Test Media for Toxicological Assessment, NIST Special Publication, 2012 1200 4.
[21] H. Kato, A. Nakamura, M. Horie, S. Endoh, K. Fujita, H. Iwahashi, S. Kinugasa, Preparation and characterization of stable dispersions of carbon black and nanodiamond in culture medium for in vitro toxicity assessment, Carbon 49 (2011) 3989–3997.
[22] T. Phenrat, N. Saleh, K. Sirk, H.-J. Kim, R.D. Tilton, G.V. Lowry, Stabilization of aqueous nanoscale zerovalent iron dispersions by anionic polyelectrolytes: adsorbed anionic polyelectrolyte layer properties and their effect on aggregation and sedimentation, J. Nanopart. Res. 10 (2008) 795–814.
[23] Q. Yangshuai, Y. Yongfu, Z. Lingyan, P. Weijun, Q. Yupeng, Dispersion and agglomeration mechanism of flaky graphite particles in aqueous solution, J. Dispersion Sci. Technol. 38 (2017) 796–800.
[24] M.P. Tong, P.T. Zhu, X.J. Jiang, H. Kim, Influence of natural organic matter on the deposition kinetics of extracellular polymeric substances (EPS) on silica, Colloid Surf. B 87 (2011) 151–158.
[25] Organization for Economic Cooperation and Development, Test No. 203: Fish, Acute Toxicity Test, OECD Publishing, 1992.
[26] Organization for Economic Cooperation and Development, Test No. 202: Daphnia Sp. Acute Immobilisation Test, OECD Publishing, 2004.
[27] H.W. Bischoff, H.C. Bold, Some Soil Algae from Enchanted Rock and Related Algal Species, University of Texas, 1963.
[28] R. Janet, E. Stein, J.R. Stein, Handbook of Phycological Methods: Culture Methods and Growth Measurements, Cambridge University Press, 1973.
[29] Organization for Economic Cooperation and Development, Test No. 201: Freshwater Alga and Cyanobacteria, Growth Inhibition Test, OECD Publishing, 2011.
[30] J. Taurozzi, V. Hackley, M. Wiesner, Preparation of Nanoscale TiO_2 Dispersions in an Environmental Matrix for Eco-Toxicological Assessment, NIST Special Publication, 2012 1200 5.
[31] Y. Zhang, Y. Chen, P. Westerhoff, J. Crittenden, Impact of natural organic matter and divalent cations on the stability of aqueous nanoparticles, Water Res. 43 (2009) 4249–4257.
[32] Z. Ma, C. Gao, J. Yuan, J. Ji, Y. Gong, J. Shen, Surface modification of poly-L-lactide by photografting of hydrophilic polymers towards improving its hydrophilicity, J. Appl. Polym. Sci. 85 (2002) 2163–2171.
[33] G. Kim, J. Choi, R.A. Silva, Y. Song, H. Kim, Feasibility of bench-scale selective bioflotation of copper oxide minerals using *Rhodococcus opacus*, Hydrometallurgy

168 (2017) 94–102.
[34] J. Choi, S.Q. Choi, K. Park, Y. Han, H. Kim, Flotation behaviour of malachite in mono-and di-valent salt solutions using sodium oleate as a collector, Int. J. Miner. Process. 146 (2016) 38–45.
[35] M. Sadiki, H. Barkai, S. Ibnsouda Koraichi, S. Elabed, The effect of the Thymus vulgaris extracts on the physicochemical characteristics of cedar wood using angle contact measurement, J. Adhes. Sci. Technol. 28 (2014) 1925–1934.
[36] K. Azelmad, F. Hamadi, R. Mimouni, K. Amzil, H. Latrache, Physicochemical characterization of *Pseudomonas aeruginosa* isolated from catering substratum surface and investigation of their theoretical adhesion, Surf. Interf. 12 (2018) 26–30.
[37] M. Van Loosdrecht, J. Lyklema, W. Norde, G. Schraa, A. Zehnder, The role of bacterial cell wall hydrophobicity in adhesion, Appl. Environ. Microbiol. 53 (1987) 1893–1897.
[38] Y. Lin, T.W. Smith, P. Alexandridis, Adsorption of a rake-type siloxane surfactant onto carbon black nanoparticles dispersed in aqueous media, Langmuir 18 (2002) 6147–6158.
[39] Y. Han, D. Kim, G. Hwang, B. Lee, I. Eom, P.J. Kim, M. Tong, H. Kim, Aggregation and dissolution of ZnO nanoparticles synthesized by different methods: influence of ionic strength and humic acid, Colloids Surf. A: Physicochem. Eng. Aspects 451 (2014) 7–15.
[40] S. Park, A. Gomez-Flores, Y.S. Chung, H. Kim, Removal of cadmium and lead from aqueous solution by hydroxyapatite/chitosan hybrid fibrous sorbent: kinetics and equilibrium studies, J. Chem. 2015 (2015).
[41] Y. Han, G. Hwang, D. Kim, S.A. Bradford, B. Lee, I. Eom, P.J. Kim, S.Q. Choi, H. Kim, Transport, retention, and long-term release behavior of ZnO nanoparticle aggregates in saturated quartz sand: role of solution pH and biofilm coating, Water Res. 90 (2016) 247–257.
[42] A.R. Petosa, D.P. Jaisi, I.R. Quevedo, M. Elimelech, N. Tufenkji, Aggregation and deposition of engineered nanomaterials in aquatic environments: role of physicochemical interactions, Environ. Sci. Technol. 44 (2010) 6532–6549.
[43] J. Gregory, Approximate expressions for retarded van der Waals interaction, J. Colloid Interf. Sci. 83 (1981) 138–145.
[44] C.J. Van Oss, Interfacial Forces in Aqueous media, CRC press, 2006.
[45] C. Van Oss, R. Good, The “equilibrium distance” between two bodies immersed in a liquid, Colloids Surf. 8 (1984) 373–381.
[46] S.A. Bradford, S. Torkzaban, Colloid transport and retention in unsaturated porous media: a review of interface-, collector-, and pore-scale processes and models, Vadose Zone J. 7 (2008) 667–681.
[47] J. Israelachvili, Intermolecular and surface forces, Intermolecular and Surface Forces, revised third edition, Elsevier Science, 2011.
[48] M.S. Mauter, M. Elimelech, Environmental applications of carbon-based nanomaterials, Environ. Sci. Technol. 42 (2008) 5843–5859.
[49] M.-L. Luo, J.-Q. Zhao, W. Tang, C.-S. Pu, Hydrophilic modification of poly (ether sulfone) ultrafiltration membrane surface by self-assembly of TiO_2 nanoparticles, Appl. Surf. Sci. 249 (2005) 76–84.
[50] Y. Kamiyama, J. Israelachvili, Effect of pH and salt on the adsorption and interactions of an amphoteric polyelectrolyte, Macromolecules 25 (1992) 5081–5088.
[51] X. Yang, S. Deng, M.R. Wiesner, Comparison of enhanced microsphere transport in an iron-oxide-coated porous medium by pre-adsorbed and co-depositing organic matter, Chem. Eng. J. 230 (2013) 537–546.
[52] L. Cai, L. Hu, H. Shi, J. Ye, Y. Zhang, H. Kim, Effects of inorganic ions and natural organic matter on the aggregation of nanoplastics, Chemosphere (2018).
[53] F.M. Omar, H.A. Aziz, S. Stoll, Aggregation and disaggregation of ZnO nanoparticles: influence of pH and adsorption of Suwannee River humic acid, Sci. Total Environ. 468 (2014) 195–201.
[54] J. Chen, Z. Xiu, G.V. Lowry, P.J. Alvarez, Effect of natural organic matter on toxicity and reactivity of nano-scale zero-valent iron, Water Res. 45 (2011) 1995–2001.
[55] A.M.E. Badawy, T.P. Luxton, R.G. Silva, K.G. Scheckel, M.T. Suidan, T.M. Tolaymat, Impact of environmental conditions (pH, ionic strength, and electrolyte type) on the surface charge and aggregation of silver nanoparticles suspensions, Environ. Sci. Technol. 44 (2010) 1260–1266.
[56] A.A. Keller, H. Wang, D. Zhou, H.S. Lenihan, G. Cherr, B.J. Cardinale, R. Miller, Z. Ji, Stability and aggregation of metal oxide nanoparticles in natural aqueous matrices, Environ. Sci. Technol. 44 (2010) 1962–1967.
[57] X. Zhu, H. Chen, W. Li, Y. He, P. Brookes, J. Xu, Aggregation kinetics of natural soil nanoparticles in different electrolytes, Eur. J. Soil Sci. 65 (2014) 206–217.
[58] E.M. Hotze, T. Phenrat, G.V. Lowry, Nanoparticle aggregation: challenges to understanding transport and reactivity in the environment, J. Environ. Qual. 39 (2010) 1909–1924.
[59] T. Phenrat, N. Saleh, K. Sirk, R.D. Tilton, G.V. Lowry, Aggregation and sedimentation of aqueous nanoscale zerovalent iron dispersions, Environ. Sci. Technol. 41 (2007) 284–290.
[60] J. Ju, X. Yao, X. Hou, Q. Liu, Y.S. Zhang, A. Khademhosseini, A highly stretchable and robust non-fluorinated superhydrophobic surface, J. Mater. Chem. A (2017).
[61] J. Marczak, M. Kargol, M. Psarski, G. Celichowski, Modification of epoxy resin, silicon and glass surfaces with alkyl-or fluoroalkylsilanes for hydrophobic properties, Appl. Surf. Sci. 380 (2016) 91–100.
[62] E.M. Hoek, G.K. Agarwal, Extended DLVO interactions between spherical particles and rough surfaces, J. Colloid Interf. Sci. 298 (2006) 50–58.
[63] J.E. Song, T. Phenrat, S. Marinakos, Y. Xiao, J. Liu, M.R. Wiesner, R.D. Tilton, G.V. Lowry, Hydrophobic interactions increase attachment of gum arabic-and PVP-coated Ag nanoparticles to hydrophobic surfaces, Environ. Sci. Technol. 45 (2011) 5988–5995.
[64] M. Tong, Y. Shen, H. Yang, H. Kim, Deposition kinetics of MS2 bacteriophages on clay mineral surfaces, Colloids Surf. B 92 (2012) 340–347.
[65] M. Elimelech, Kinetics of capture of colloidal particles in packed beds under attractive double layer interactions, J. Colloid Interf. Sci. 146 (1991) 337–352.
[66] M. Ramos-Tejada, A. Ontiveros, J. Viota, J. Durán, Interfacial and rheological properties of humic acid/hematite suspensions, J. Colloid Interf. Sci. 268 (2003) 85–95.
[67] K.-Y. Law, H. Zhao, Surface Wetting: Characterization, Contact Angle, and Fundamentals, Springer, 2015.
[68] K.-Y. Law, Definitions for Hydrophilicity, Hydrophobicity, and Superhydrophobicity: Getting the Basics Right, ACS Publications, 2014.
[69] M. Hermansson, The DLVO theory in microbial adhesion, Colloids Surf. B 14 (1999) 105–119.
[70] J.J. Valle-Delgado, J.A. Molina-Bolívar, F. Galisteo-Gonzalez, M.J. Gálvez-Ruiz, A. Feiler, M.W. Rutland, Interaction forces between BSA layers adsorbed on silica surfaces measured with an atomic force microscope, J. Phys. Chem. B 108 (2004) 5365–5371.
[71] B. Derjaguin, N. Churaev, The current state of the theory of long-range surface forces, Colloids Surf. 41 (1989) 223–237.
[72] K.L. Chen, M. Elimelech, Influence of humic acid on the aggregation kinetics of fullerene (C_{60}) nanoparticles in monovalent and divalent electrolyte solutions, J. Colloid Interf. Sci. 309 (2007) 126–134.
[73] E.K. Fauss, R.I. MacCuspie, V. Oyanedel-Craver, J.A. Smith, N.S. Swami, Disinfection action of electrostatic versus steric-stabilized silver nanoparticles on *E. coli* under different water chemistries, Colloids Surf. B 113 (2014) 77–84.
[74] F. Loosli, P. Le Coustumer, S. Stoll, Effect of natural organic matter on the disagglomeration of manufactured TiO_2 nanoparticles, Environ. Sci.: Nano 1 (2014) 154–160.
[75] B. Xie, Z.H. Xu, W.H. Guo, Q.L. Li, Impact of natural organic matter on the physicochemical properties of aqueous C_{60} nanoparticles, Environ. Sci. Technol. 42 (2008) 2853–2859.
[76] S.A. Bradford, S. Torkzaban, Colloid interaction energies for physically and chemically heterogeneous porous media, Langmuir 29 (2013) 3668–3676.
[77] S.A. Bradford, H. Kim, C. Shen, S. Sasidharan, J. Shang, Contributions of nanoscale roughness to anomalous colloid retention and stability behavior, Langmuir 33 (2017) 10094–10105.
[78] H. Ma, C.J. Winslow, B.E. Logan, Spectral force analysis using atomic force microscopy reveals the importance of surface heterogeneity in bacterial and colloid adhesion to engineered surfaces, Colloids Surf. B 62 (2008) 232–237.
[79] S.A. Bradford, S. Sasidharan, H. Kim, G. Hwang, Comparison of types and amounts of nanoscale heterogeneity on bacteria retention, Front. Environ. Sci. 6 (2018) 56.